Interactive Visual Analysis of Perfusion Data

Steffen Oeltze, Helmut Doleisch, Helwig Hauser, Philipp Muigg, and Bernhard Preim

Abstract—Perfusion data are dynamic medical image data which characterize the regional blood flow in human tissue. These data have a great potential in medical diagnosis, since diseases can be better discriminated and detected at an earlier stage compared to static image data. The wide-spread use of perfusion data is hampered by the lack of efficient evaluation methods. For each voxel, a time-intensity curve characterizes the enhancement of a contrast agent. Parameters derived from these curves characterize the perfusion and have to be integrated for diagnosis. The diagnostic evaluation of this multi-field data is challenging and time-consuming due to its complexity. For the visual analysis of such datasets, feature-based approaches allow to reduce the amount of data and direct the user to suspicious areas.

We present an interactive visual analysis approach for the evaluation of perfusion data. For this purpose, we integrate statistical methods and interactive feature specification. Correlation analysis and Principal Component Analysis (PCA) are applied for dimension reduction and to achieve a better understanding of the inter-parameter relations. Multiple, linked views facilitate the definition of features by brushing multiple dimensions using non-binary and composite brushes. The specification result is linked to all views establishing a focus+context style of visualization in 3D. We discuss our approach with respect to clinical datasets from the three major application areas: breast tumor diagnosis, ischemic stroke diagnosis as well as the diagnosis of the coronary heart disease (CHD). It turns out that the significance of perfusion parameters strongly depends on the individual patient, scanning parameters and data pre-processing.

Index Terms—Multi-field Visualization, Visual data mining, Time-varying volume data, Integrating Infovis/Scivis

1 Introduction

Compared to static image data, where the morphology of anatomic and pathological structures is represented with high spatial resolution, dynamic image data characterizes functional processes, such as metabolism and blood flow, which is often essential to detect diseases at an early stage or to discriminate pathologies with very similar morphology. Important examples of dynamic medical image data are functional MRI, where activations of brain areas are measured, dynamic SPECT, where metabolic processes are imaged and perfusion imaging, where the blood flow is represented. We focus on perfusion data which are acquired to support essential diagnostic tasks, e.g., cerebral perfusion for stroke diagnosis, the assessment of different types and stages of tumors, and perfusion of the myocardium (heart muscle) for CHD diagnosis.

In perfusion imaging, the distribution of contrast agents (CA) is registered to assess blood flow and tissue kinetics. For each voxel, a time-intensity curve characterizes the CA enhancement. How long it takes until the maximum amount of CA is delivered, which maximum is achieved as well as other parameters are derived from these curves for medical diagnosis.

The derived parameters represent a special instance of multi-field data which is becoming more and more important in medicine [13], [5]. They are substitutes for physiological parameters such as tumor perfusion and vessel permeability [7]. The integrated analysis of several parameters in a suspicious region is essential. For the diagnosis of ischemic stroke, e.g., if the blood flow is delayed in a particular region, it is crucial to evaluate if the overall blood flow is also reduced [20].

To streamline the integrated analysis of perfusion parameters, we present a visual analysis approach incorporating pre-processing and statistical methods as well as feature specification steps. Motion correction and noise reduction are fundamental pre-processing issues to achieve a reliable correspondence of voxels over time. Since the different parameters are derived from the same time-intensity curve that characterizes the CA enhancement, it is likely that some parameters correlate with each other. We apply a correlation analysis and a PCA to achieve a better understanding of the inter-parameter relations and to simplify and to speed-up the diagnosis by reducing the complexity of the multi-field data. Besides its complexity, the non-standardized parameter domain which depends on the scanning protocol complicates the diagnostic evaluation. For the visual analysis of such data, feature-based approaches allow to direct the user to suspicious regions and to reduce the amount of data to a representative subset. Our approach integrates methods for interactive feature specification of high-dimensional complex features in multi-field data. Multiple, linked views facilitate the definition of features which can be complex and/or hierarchically described by brushing multiple dimensions. Non-binary brushes account for the uncertainty involved in the inspection of a non-standardized parameter domain. Furthermore, they represent a natural mapping of irreversibly damaged or malignant tissue, suspicious or reversibly damaged tissue and healthy tissue to focus, near-focus and context. The specification result from all views is linked to a 3D-view, establishing a focus+context style of visualization. The 3D-representation of the perfusion parameters within their anatomic context allows a localization of the specification result.

Our visual analysis approach primarily addresses medical researchers seeking for a better understanding of which perfusion parameters are crucial for specific diagnostic tasks and how imaging parameters influence the expressiveness of perfusion parameters. This research is motivated by contradictory recommendations in medical research papers, e.g., [2] and [30] for CHD diagnosis.

This paper is structured as follows: In Sec. 2, we give an overview on the medical background in perfusion diagnosis and on correlation analysis and PCA. In Sec. 3, we describe our analysis approach. The application of the approach to clinical perfusion datasets from breast tumor diagnosis, ischemic stroke diagnosis, and CHD diagnosis, is discussed in Sec. 4. Prior and related work on the application of InfoVis techniques for the analysis of multi-field data as well as on the visual analysis of perfusion data are presented in Sec. 5. The last section will summarize and conclude the paper.

2 Medical and Technical Background

This section gives a brief overview on the medical background in perfusion diagnosis and further acquaints the reader with the basics of correlation analysis and PCA.

- *Steffen Oeltze and Bernhard Preim are with the Department of Simulation and Graphics, University of Magdeburg, Magdeburg, Germany, E-mail: {stoeltze|preim}@isg.cs.uni-magdeburg.de.*
- *Helmut Doleisch and Philipp Muigg are with the VRVis Research Center, Vienna, Austria, E-mail: {Doleisch|Muigg}@VRVis.at.*
- *Helwig Hauser is with the Department of Informatics, University of Bergen, Bergen, Norway, E-mail: Helwig.Hauser@uib.no.*

2.1 Perfusion Diagnosis

In perfusion imaging, a CA is injected intravenously and its distribution is measured by a repeated acquisition of subsequent images covering the volume of interest. The CA provides signal changes in the acquired 4D-data (3D+time). In case of a perfusion defect, the corresponding region exhibits an abnormal change in signal intensities. The spatial resolution and quality of perfusion data are worse than those of static data. High temporal resolution can only be achieved at the expense of lower spatial resolution and image quality.

Particularly CT, PET, SPECT and MRI data are employed for perfusion imaging. In the following, we only consider MR perfusion since MRI is the most widespread perfusion imaging technique for breast tumor diagnosis, it outperforms CT in stroke diagnosis since the entire brain can be scanned (instead of a single slice with CT) and it has shown to have at least a similar sensitivity and specificity in comparison to PET and SPECT in CHD diagnosis. T1-weighted MR images are typically used for breast tumor diagnosis, whereas T2-weighted MR images are employed for the diagnosis of ischemic stroke. In T1-weighted imaging, a signal enhancement is achieved in areas of contrast agent accumulation. On the other hand, T2-weighted images lead to a decrease of signal intensity where the CA accumulates.

Perfusion Parameters. For the diagnosis, regions of interest in healthy and suspicious tissue are defined, and time-intensity curves – averaged over all voxels in the selected region – are analyzed. Depending on the application area, different sets of parameters, derived from the curves, are relevant. However, some parameters are of general interest for almost all application areas (see Fig. 1). Before we describe these parameters, we introduce three parameters necessary for a reliable evaluation.

The *CA arrival* represents the point in time when the signal enhancement actually starts, whereas $Time_{End}$ refers to the end of the first CA passage. The *Baseline* represents the average intensity before *CA arrival* (see Fig. 1). These parameters are determined to focus the evaluation of the time-intensity curve to the relevant portion.

Assessing perfusion considering the actual *CA arrival*, $Time_{End}$ and the *Baseline* is essential to compare perfusion analysis results from different scanning devices and patients. Major diagnostically relevant perfusion parameters are:

- *Peak Enhancement (PE)*. The maximum value (between *CA arrival* and $Time_{End}$) normalized by subtracting the *Baseline*. The *PE* separates the time interval between *CA arrival* and $Time_{End}$ into a phase of CA *wash-in* followed by the CA *wash-out*.

- *Time To Peak (TTP)*. The point of time where *PE* occurs, normalized by subtracting *CA arrival* time. This parameter allows to assess whether the blood supply is delayed in a particular region.

- *Integral*. For a certain time interval (often representing one cycle or pass of blood flow) the area between the curve and the *Baseline* – the approximated integral – is computed. Together, *PE* and *Integral* may give a hint on reduced blood flow.

- *Mean Transit Time (MTT)*. In the time interval used for the integral calculation, MTT specifies the first momentum of the curve. It is normalized by subtracting *CA arrival* time.

- The *Slope* characterizes the steepness of the curve during wash-in. Depending on the temporal resolution, different regression methods are used to characterize the curve progression. The term *Up-Slope* in cardiac diagnosis relates to the maximum slope between two or three subsequent time-steps between *CA arrival* and TTP. In tumor perfusion studies, the related parameter *MiTR* (Maximum intensity to Time Ratio) is determined; it is computed as PE/TTP and it is thus an average slope in the interval between *CA arrival* and TTP.

- The *DownSlope* characterizes the steepness of the descending curve during wash-out and is computed similar to the $Slope$.

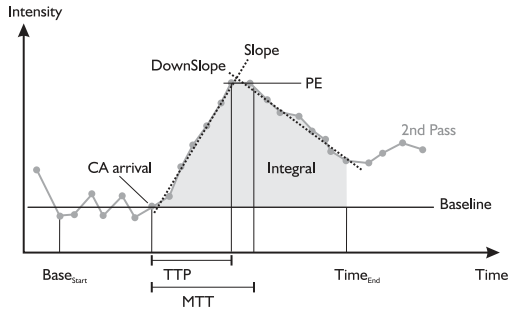

Fig. 1. A typical time-intensity curve in myocardial perfusion with a significant first pass and an alleviated second pass of contrast agent traversal annotated with the essential parameters to evaluate the first pass. Similar curves are observed in cerebral perfusion.

The parameters are derived per voxel and stored in separate *parameter volumes* (3D). As a major pre-processing step, noise reduction is often solved by conventional noise reduction filters, such as Gaussian. Lysaker et al. [24] introduced a filter for 4D data that better preserves features based on partial differential equations, which simulate a diffusion process. Motion-correction is the second major pre-processing task, carried out to establish a valid inter-pixel correspondence. Motion correction is essential when breathing, heartbeat, patient movement, or muscle relaxation occurs. The motion correction algorithm developed by Rueckert et al. is widely used [31].

2.2 Correlation and Principal Component Analysis

Correlation analysis reveals whether variables vary independently of each other or are (inversely) proportional. The amount of correlation is represented by the so-called *correlation coefficient (r)*. In the following, we assume a matrix $A^{m\times n}$ representing n variables (perfusion parameters) and m observations (voxels of the *parameter volumes*). The symmetric matrix $R^{n\times n}$ of correlation coefficients is then computed based on the covariance matrix C of A. A value of $r_{ij} = -1$ indicates a perfect inversely proportional relationship, whereas a value of $r_{ij} = 1$ corresponds to a perfect proportional relationship. A value of $r_{ij} = 0$ relates to non-correlated variables. Besides R, an equally-sized symmetric matrix P of p-values is computed for testing the hypothesis of no correlation. If a particular p-value is < 0.05, the correlation is considered significant. Müller et al. [26] suggest that the user may exclude variables from a PCA that strongly correlate with each other. Otherwise, these variables might misleadingly strengthen certain trends.

The PCA is a technique from multivariate statistics to detect variables from multi-dimensional data that may be redundant. For the purpose of dimension reduction, these variables may be grouped together to form a new variable. Furthermore, PCA explains the structure of relationships between variables and thus provides additional insight into the data. The PCA results in new variables, the so-called *principal components*. Each principal component (pc) represents a single axis in a new orthogonal coordinate space (*pc-space*) – generated by a variance maximum rotation of the original data space. The first pc ($pc1$) explains most of the variance in the original data, the second one ($pc2$) most of the remaining variance, and so on.

Before applying a PCA, it is often reasonable to standardize the data. This is necessary, when the variables were not measured in the same units or when their variance is substantial. For standardization, A is centered around its mean and then each column of A is divided by its standard deviation. This step is often referred to as *Auto-scaling*. One way to compute the pc's is to apply a *Singular Value Decomposition (SVD)*. As a result, the SVD returns matrices $PCS^{n\times n}$, $scores^{m\times n}$ and a vector containing the eigenvalues $\lambda^{1\times n}$ of C. Each column of PCS consists of n *loadings* representing the weights for the linear combination of the n original variables. The *scores* are the coordinates of the original data transformed into $pc-space$. The vector λ represents the variances explained by the n pc's.

According to Müller et al. [26], the PCA results may be exploited

in several ways, e.g., to detect prominent trends in the data. These trends are represented by the pc's. The *loadings* indicate how individual variables correlate with these trends. The eigenvalues of C may be applied to neglect less significant trends during the analysis (low values correspond to a low variance explained by the corresponding pc). A major problem involved in interpreting PCA results is the difficulty to relate trends to the original variables [26]. Therefore, Müller et al. [26] suggest to oppose the *scores* and the original variables in a scatterplot. Another approach they recommend is to present the *scores* in their spatial frame of reference (the original perfusion data). Furthermore, linking & brushing should be applied to relate the *scores* to the original variables.

3 A Perfusion Data Analysis Approach

This section describes the visual analysis approach independent of a specific application area. However, the included figures have been generated based on cerebral perfusion data to illustrate the approach by means of a real-world example (see Sec. 4.1).

The approach consists of three major components (see Fig. 2): a pre-processing component, a component for statistical analysis and a component for interactive feature specification in multi-field data. For this paper, these components have each been implemented in Me*VisLab*[1], a platform for medical image processing and visualization, *MATLAB*[2] and the framework *SimVis*[3].

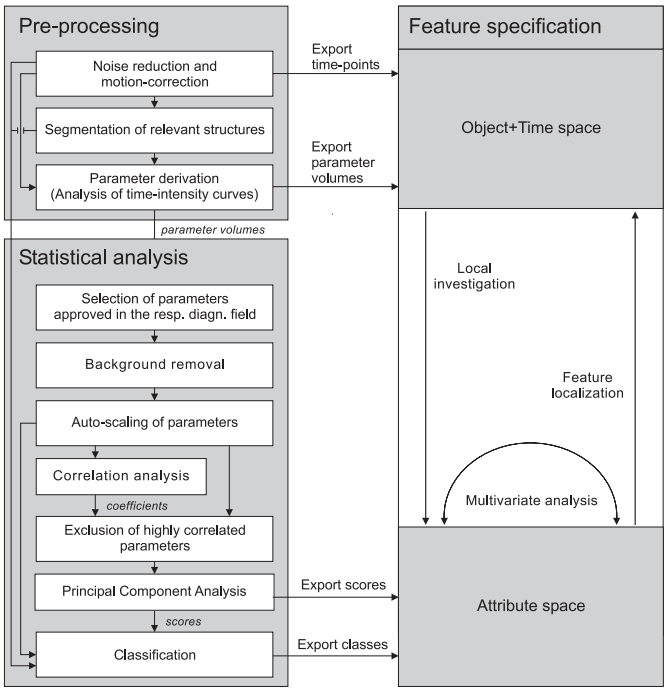

Fig. 2. A perfusion data analysis approach consisting of three components: pre-processing, statistical analysis and interactive feature specification.

3.1 Pre-processing

The original 4D-perfusion data serves as input for the pre-processing component. Here, the data is noise reduced applying a Gaussian kernel and motion-corrected according to [31] (see Sec. 2.1). Next, the separate time-points (3D-data) are exported and may serve, e.g., as context information during the visual analysis.

[1]Product of the MeVis Research; www.mevislab.de
[2]Product of the MathWorks, Inc.; www.mathworks.com
[3]Developed by the VRVis, Vienna; www.simvis.at

For some applications, such as ischemic stroke or CHD diagnosis, it is useful to restrict the computation of perfusion parameters to relevant structures (brain tissue or ventricles of the heart). A variety of segmentation algorithms has been integrated into Me*VisLab*, e.g., a fast watershed algorithm for brain segmentation [14]. Once the relevant structures have been segmented, the perfusion parameters are derived voxel-wise for these regions and exported separately as *parameter volumes*. The *parameter volumes* serve as input for the feature specification as well as for the statistical component. The segmentation part may be skipped if the entire dataset must be analyzed.

3.2 Statistical Analysis

At the beginning of the statistical analysis, the user is presented a list containing the perfusion parameters which have been approved in his or her diagnostic field of interest (see Sec. 4.1-4.3). The user may refine this initial set resulting in a new set $\{P_k\}$ of k parameters. In a next step, the background voxels within the *parameter volumes* corresponding to $\{P_k\}$ are identified to restrict further computations to the anatomic structures. Based on the histogram of one of these *parameter volumes*, the background voxels are identified (the highest peak in the histogram) and excluded from further analysis (*Background removal*). The decision may be refined by defining a threshold. The indices of the remaining m voxels VOX_{relev} are stored in a vector ID_{relev}. Then, the perfusion parameter matrix $A^{m\times k}$ is constructed considering only the voxels referred to by ID_{relev}. As discussed in Sec. 2.2, the PCA may require a standardization of its input to deliver meaningful results. Since the perfusion parameters have not been measured in the same units, *Auto-scaling* is applied to A. The result of this step is referred to as $A_{std}^{m\times k}$.

To evaluate the relationship between several parameters, a correlation analysis is carried out resulting in matrices R and P. In order to consider only significant correlations, P is examined for values < 0.05. The correlation coefficients in R corresponding to the remaining values are set to 0 (no correlation). A visual representation of R now enables the user to identify parameters that are highly correlated (see Fig. 3). A scatterplot matrix is generated by plotting all columns in A_{std} against each other. The diagonal of the scatterplot matrix shows the histogram of each parameter. The background color of each plot has been chosen according to the respective value in R. A color scale has been designed that visually separates negative and positive coefficients. Furthermore, it emphasizes correlation coefficients < -0.9 or > 0.9. When dragging the mouse over the plots, the respective correlation coefficient is displayed. Zooming in and out enables the user to further explore separate plots. The visualization of R in Fig. 3 shows the following strong correlations: $Integral \leftrightarrow PE$, $PE \leftrightarrow MiTR$, $PE \leftrightarrow Slope$, $Slope \leftrightarrow MiTR$ *and* $Slope \leftrightarrow DownSlope$ (inversely proportional). Since parameters *PE* and *Slope* strongly correlate with three other parameters, respectively, they may be excluded from further processing. This results in the Matrix $A_{corr}^{m\times l}$, where l is the number of remaining parameters.

In a next step, a PCA is carried out based on A_{corr} resulting in the matrices $PCS^{l\times l}$, $scores^{m\times l}$ and a vector $\lambda^{1\times l}$ (recall Sec. 2.2). To detect trends in the pc's, the *loadings* in *PCS* are visualized in a vertical bar chart (see Fig. 4 (left)). However, the PCA does not only reveal the trends but it orders them by their significance – expressed by the variances in λ. To incorporate this significance in the visualization, the *loadings* in column $i, i \in [1,l]$ of *PCS* are weighted with $\lambda(1,i)$ according to [26] (see Fig. 4 (right)). The plot in Fig. 4 (right) reveals a major trend represented by $pc1$. This trend is determined by the parameters *Integral*, *DownSlope* and *MiTR*. The positive *loadings* of *Integral* and *MiTR* indicate a direct proportional relationship, whereas the negative *loading* of *DownSlope* indicates an inversely proportional relationship. A second and a third trend are respectively observed in $pc2$ and $pc3$. To relate the trends to the original perfusion parameters, the *scores* are exported for later processing within the feature specification component.

The end of the statistical analysis constitutes a classification step. This step has not yet been implemented and will therefore not be discussed in the paper. However, related work indicates that in particular,

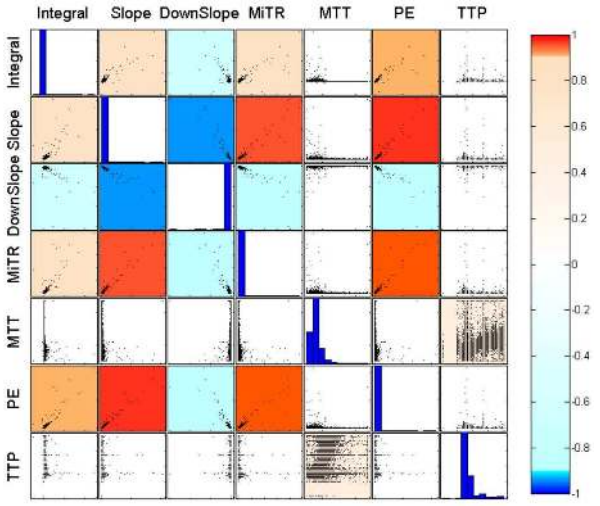

Fig. 3. Scatterplot matrix of perfusion parameters. The background color of each plot is chosen according to the respective correlation coefficient. The color scale is designed such that coefficients < -0.9 or > 0.9 are emphasized. The diagonal of the matrix shows a histogram for each parameter.

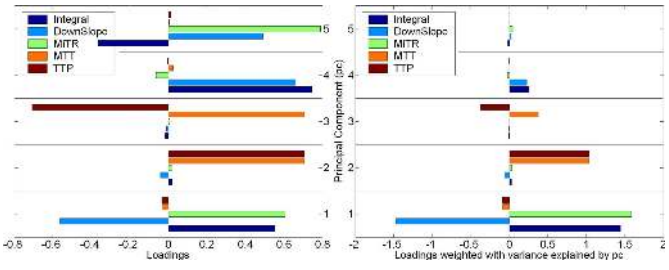

Fig. 4. Principal components and their *loadings* for each of the relevant parameters (left). To incorporate the significance of each trend, the *loadings* are weighted with the variance explained by the corresponding pc (right).

techniques to classify Dynamic Contrast-Enhanced MRI Mammography (DCE-MRIM) data are promising in detecting suspicious regions (see Sec. 5). Hence, the statistical analysis incorporates a classification of the (pre-processed) perfusion data – possibly restricted to relevant structures–, of the standardized perfusion parameters and of the *scores*. The detected classes are exported and may be processed within the feature specification component.

3.3 Feature Specification

The interactive feature specification of data coming from the preprocessing as well as from the statistical analysis stage of our approach is carried out in a framework employing the SimVis technology [11][10]. SimVis was previously developed for the analysis of 3D time-dependent flow simulation data, but has recently been extended to also cope with multiple other data types, e.g., measured 3D weather radar data. Here, we extended the technology further to also work with time-dependent multi-field data from medical applications.

In SimVis, multiple linked views are used to concurrently show, explore and analyze different aspects of multi-field data. 3D views of the volume (also over time) can be used next to several types of attribute views, e.g., scatterplots or histograms. Interactive feature specification is usually performed in these attribute views. The user chooses to visually represent selected data attributes in such a view, thereby gaining insight into the selected relations within the data. Then, the interesting subsets of the data are interactively brushed directly on the screen (compare to the XmdvTool [34] and see Fig. 5(b) for an example). The result of such a brushing operation is reintegrated within the data in the form of a synthetic data attribute $DOI_j \in [0,1]$ (*degree of interest (DOI) attribution* of the data, compare to Furnas [12]). This DOI attribution is used in the 3D views of the analysis setup to visually discriminate the interactively specified features from the rest of the data in a focus+context visualization style which is consistent in all (linked) views [15].

In the SimVis system *smooth brushing* [11] (enabling fractional DOI-values) as well as the logical combination of brushes for the specification of *complex features* [10] are supported. A smooth brush results in a trapezoidal DOI function around the main region of interest in the attribute views. To enable the integration of a fully flexible derived data concept, a data calculator module with a respective graphical user interface has been added. New attributes can be derived from existing ones and thereafter are available for full investigation in all linked views.

There are several different purposes of the interactive feature specification process and the resulting exploration and analysis steps, of which the most important are:

- *Feature localization*: to search for places in the 3D domain of the data where certain feature characteristics are present. In the SimVis approach, the user can brush features in attribute views and concurrently localize the respective feature in the 4D (3D+time) volume domain.
- *Multi-variate analysis*: to investigate multi-variate data properties by specifying a feature in one attribute view and at the same time analyzing the DOI distribution with respect to other data attributes in other attribute views (through view linking).
- *Local investigation*: to inspect the values of selected data attributes with respect to certain spatiotemporal subsets of the 3D volume domain. In the SimVis system, the user can also load spatial as well as temporal data references into attribute views – brushing these kinds of data attributes then yields features which are specified according to their spatiotemporal extents.

4 Application

The perfusion data analysis approach introduced in Sec. 3 has been applied to 5 datasets so far (1 from ischemic stroke diagnosis, 2 from breast tumor diagnosis and 2 from CHD diagnosis). These datasets are representative for the respective diagnostic field concerning spatial and temporal resolution. Due to space restrictions, not all analysis results can be discussed here. Therefore, the reader is referred to the following website: *wwwisg.cs.uni-magdeburg.de/cv/VAoPD/*. It contains additional analysis results, high-resolution versions of all images included in this paper and a video to illustrate the interactive aspect of the analysis.

Pre-processing. All datasets have been noise-reduced applying a Gaussian kernel. To reduce motion artifacts, the datasets from breast tumor and CHD diagnosis have been motion-corrected according to [31]. To restrict the motion-correction on the myocardium in CHD diagnosis, the datasets have been cropped before. In the dataset from ischemic stroke diagnosis, the brain tissue has been segmented by means of a watershed-algorithm [14] to restrict the parameter derivation to interesting regions. Since the T2-weighted datasets from cerebral perfusion lead to a decrease of signal intensity where the CA accumulates, the time-intensity curves appear mirrored on the *Baseline* with respect to Fig. 1. To achieve a consistent way of analyzing datasets from different application areas throughout the paper, the intensity-values were inverted. In the datasets from CHD diagnosis, the myocardium has been semi-automatically segmented in each slice by means of a live-wire technique [32]. The resulting contours have been propagated over all time-points. The final parameter derivation has been restricted to the segmentation results.

4.1 Ischemic Stroke Diagnosis

In case of an ischemic stroke, the existence and the extent of "tissue at risk" surrounding the core of the stroke has to be evaluated. Sur-

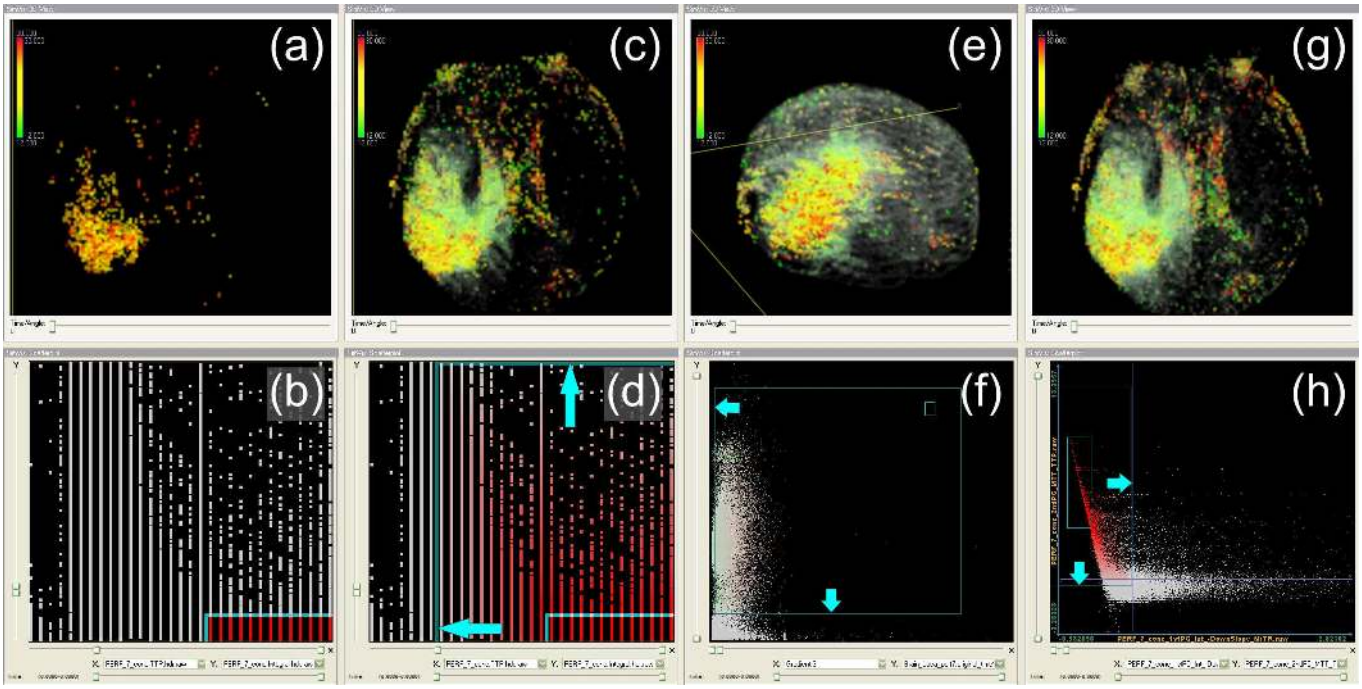

Fig. 5. Visual analysis in ischemic stroke diagnosis. In *(b)*, parameters TTP (x-axis) and $Integral$ (y-axis) have been opposed. High TTP- and low $Integral$-values (delayed and diminished perfusion) have been brushed in the scatterplot. As a result, the infarction core is revealed in *(a)* applying TTP for color-coding. Smooth brushing along both axis of the plot *(d)* gives a hint on the location of "tissue at risk" (greenish area in *(c)*). Here, the perfusion is delayed as well however, enough blood arrives over time. In *(e)*, the brain is rotated to gain a better impression of the over-all extension of the infarction in 3D. Furthermore, the shape of the brain is indicated by a smooth brushing *(f)* applied on the gradient magnitude computed from a single time-point of the perfusion data. Interestingly, a smooth brushing *(h)* in a scatterplot opposing the $scores$ for $pc1$ (x-axis) and $pc2$ (y-axis) yields a very similar result *(g)* compared to *(c)*.

gical and medicamentous interventions may salvage at least parts of the "tissue at risk" [9]. In cerebral perfusion, the *first-pass* of the CA (see Fig. 1) through the vessel components is observed. The volume of blood in each voxel is diagnostically relevant. It is measured by the *Integral* of the enhancement curve. Other approved parameters describing the cerebral blood flow are *PE, TTP, MTT* and *Slope* [21].

Case Study. The patient whose dataset will be analyzed here, suffered from an infarction in the right hemisphere (which will appear left in all subsequent images). The dataset matrix is: 128×128, slice distance: 7 mm, number of slices: 12, temporal resolution: 40 measurements in 80 seconds.

Statistical analysis. The results of the statistical analysis are illustrated in Fig. 3-4. First, the initially suggested set of approved parameters has been refined by adding *DownSlope* and *MiTR*. The examination of the correlation coefficients of the refined set revealed three types of strong correlations (recall Sec. 3.2): correlations between parameters describing the amount of blood that arrives at a certain region ($Integral \leftrightarrow PE$), between parameters describing the velocity of the enhancement ($Slope \leftrightarrow MiTR$, $Slope \leftrightarrow DownSlope$) and in between these two types ($PE \leftrightarrow MiTR$, $PE \leftrightarrow Slope$). The correlation between *Slope* and *DownSlope* is inversely proportional. Since the *DownSlope* is measured in negative values, this indicates that a fast wash-in (high *Slope*-values) is likely to be followed by a fast wash-out (high negative *DownSlope*-values). Since the parameters *PE* and *Slope* strongly correlate with three other parameters, respectively, they have been excluded from further processing.

The PCA showed four major trends ($pc1$-$pc4$) which account for $52\% + 29\% + 11\% + 7\% = 99\%$ of the variance in the data. A problem when interpreting PCA results is to assign a meaning to the newly generated coordinate axes. This has an impact, e.g., on brushing in the newly generated coordinate space. According to Müller et al. [26], we label the axes with respect to the parameters that determine the trend in the respective pc. More abstract labels could be "Amount and Velocity" for $pc1$ and "Time to Enhancement" for $pc2$.

Two interesting trends are revealed by $pc3$ and $pc4$ which conflict with $pc2$ and $pc1$, respectively (see Fig. 4). The first two pc's again describe parameter relationships which are to be expected in cerebral perfusion, whereas $pc3$ and $pc4$ characterize atypical behavior. Hence, their corresponding *scores* have been analyzed within the feature specification component. The results are illustrated on the website.

Visual analysis. A crucial task in stroke diagnosis is to localize the infarction core and especially the surrounding "tissue at risk". The first three columns in Fig. 5 illustrate how visual analysis may guide this process. In a scatterplot, TTP (x-axis) and $Integral$ (y-axis) are opposed and a region is brushed that indicates delayed and diminished perfusion (Fig. 5 (b)). As a result of this *feature localization*, the infarction core appears as a bright region (Fig. 5 (a)). High TTP-values are mapped to colors from yellow to red. Smooth brushing in both dimensions now gives a hint on the existence of "tissue at risk" (Fig. 5 (d)). A near-focus region is defined (blue arrows point at its borders) that incorporates areas where the perfusion is delayed as well, however, enough blood arrives over time. Candidate areas for "tissue at risk" appear greenish (medium TTP-values) in Fig. 5 (c). This observation could be successfully validated with [19] where the same dataset has been examined. In Fig. 5 (e), the brain has been rotated to gain a better impression of the over-all extension of the infarction in 3D. Furthermore, the shape of the brain is indicated as context information. Latter has been achieved by a smooth brushing of the gradient magnitude computed based on the intensity values from a single time-point of the original perfusion data (Fig. 5 (f)). The focus has been defined such that a smooth brushing assigns small DOI values to the majority of gradient magnitudes resulting in just a slight indication of the anatomical context. This technique will be used throughout the paper. In Fig. 5 (h), $pc1$ (x-axis) and $pc2$ (y-axis) have been opposed. As discussed above, abstract axes labels could be "Amount and Velocity" and "Time to Enhancement". Hence, small values on the x-axis and high values on the y-axis are brushed. The near-focus region is selected accordingly (blue arrows). A comparison of Fig. 5 (g) and

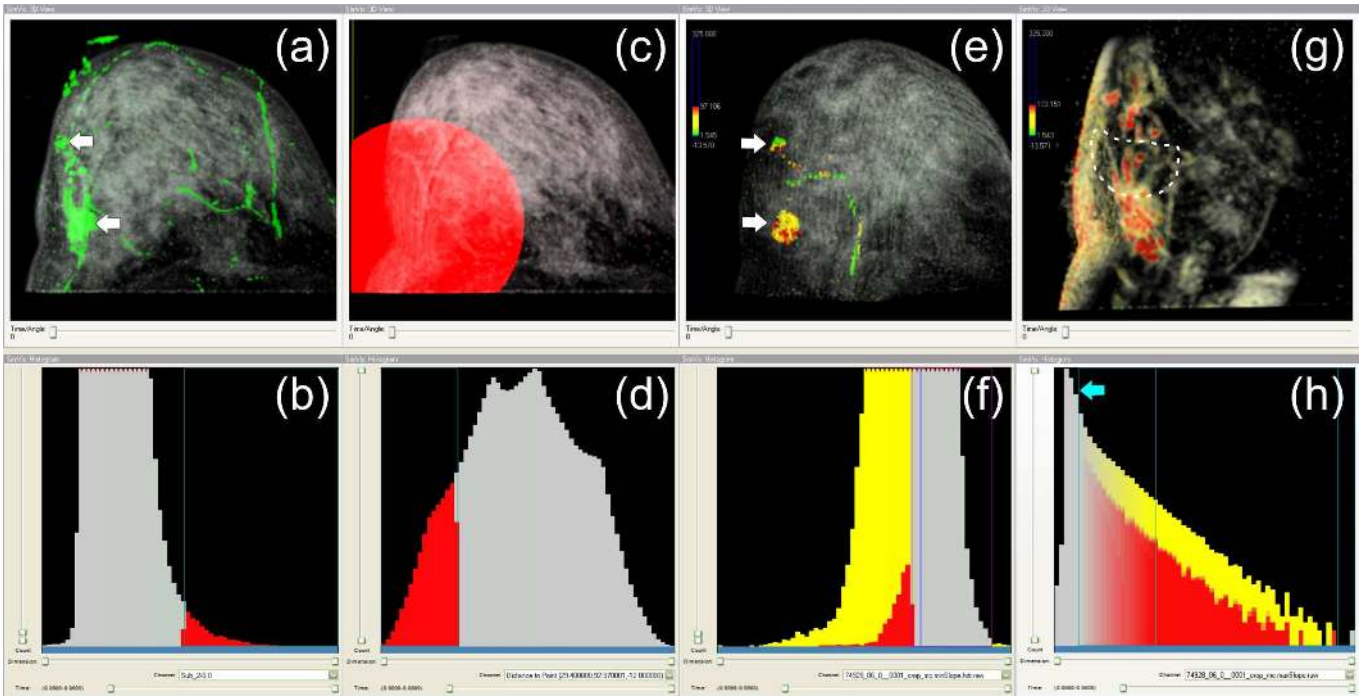

Fig. 6. Visual analysis in breast tumor diagnosis. Selection of high intensity differences between original time-points t_2 and t_0 (b) emphasizes areas were the CA is absorbed (a). Two suspicious regions are detected (arrows). The analysis is focused on a local region *LR* around S_{large} *(c)* by means of brushing small Euclidian distances between its center and the surrounding tissue *(d)*. Areas exhibiting a rapid wash-out are selected in a histogram depicting $DownSlope$ (f). A negative brush is used to exclude positive and small negative values. The corresponding areas are visualized in (e) and color-coded according to $Slope$. Yellow to red areas indicate a rapid wash-in and wash-out. A smooth brushing of $Slope$ within *LR* (h) reveals subtle jags along the border of S_{large} (g) which are typical for malignant structures.

Fig. 5 (c) shows that the revealed areas match closely. Hence, the trends expressed by $pc1$ and $pc2$ together describe CA enhancement patterns that are typical in cerebral perfusion.

4.2 Breast Tumor Diagnosis

The major diagnostic task in breast tumor diagnosis is to confirm or reject the hypothesis of a tumor being malignant. Evaluating the shape of the time-intensity curves has been proven to be effective in the differentiation of enhancing lesions [22]. Parameters that describe the shape are *MTT, MiTR, PE, Slope, DownSlope, TTP* and *Integral*. Curves – which show a rapid wash-in followed by a rapid wash-out, i.e., a significant decrease of signal intensity afterwards – are especially suspicious because they indicate strong perfusion and high permeability of vessels. Less suspicious are those curves showing a plateau later on, or those regions which continue to enhance.

Case Study. The described dataset was acquired to examine a suspicious region in the right mamma that has been detected during conventional mammography. The dataset matrix is: 458×204, slice distance: 3 mm, number of slices: 26, temporal resolution: 6 measurements in 10 minutes. In breast tissue, contrast enhancement lasts considerably longer than in cerebral blood vessels. Therefore, longer acquisition times are employed. The reduced temporal resolution allows a significant increase in spatial resolution. Due to space restrictions, the analysis results of a second DCE-MRIM dataset will only be presented on our website (*wwwisg.cs.uni-magdeburg.de/cv/VAoPD/*).

Statistical analysis. In addition to the initially suggested set of approved parameters two extra parameters have been added describing the steepness of the curve during wash-in and wash-out. Each of them was computed between two particular time-points selected by the user. The examination of the correlation coefficients revealed a strong correlation between *Integral* and *PE* as well as between *PE* and *Slope*. Since *PE* strongly correlates with two other parameters, it has been excluded from further processing. The PCA showed four major trends expressed by $pc1$-$pc4$. All together account for $\approx 91\%$ of the variance in the data. Further details on the interpretation of the pc's is available on the website. In the following, the focus is on a streamlined localization and separation of suspicious structures for local investigation.

Visual analysis. Subtraction images emphasize regions where the CA is absorbed (see Sec. 5). Hence, additional parameters have been derived based on the original time-points in the perfusion data. Each parameter describes the intensity difference between two subsequent time-points t_j and t_i, where $j > i$. In Fig. 6 (b), high differences in intensity between time-points t_2 and t_0 have been selected ($Selection1$). The corresponding areas are emphasized in Fig. 6 (a). The structure S_{large} which has already been detected in conventional mammography, is pointed at by the lower arrow. Furthermore, a smaller structure S_{small} is revealed close to the thoracic wall (upper arrow). Besides these areas, major vessels and the acromastium are emphasized. To focus the analysis on an area around S_{large} for *local investigation*, the Euclidean distance between its center and the surrounding tissue is computed. Then, a range of distance values ($Selection1_1$) within $Selection1$ is brushed (Fig. 6 (d)) such that the local region *LR* around S_{large} includes S_{small} (Fig. 6 (c)). In (Fig. 6 (f)), $Selection1_1$ (red bars) is visualized within a histogram of parameter *DownSlope* for *multivariate analysis*. High negative values indicating a rapid wash-out of the CA are typical for malignant tumors. Hence, this range has been selected within $Selection1_1$ by excluding positive and small negative values with the help of a negative brush (the blue line marks the vertical zero-axis). The result is color-coded by means of parameter *Slope* in Fig. 6 (e). S_{large} and S_{small} both exhibit a rapid wash-in and wash-out and are thus likely to be malignant. S_{small} partially shows small *Slope* values which should be further investigated. Another indication that confirms the suspicion of malignancy is illustrated in Fig. 6 (g-h). A smooth brushing of high and medium *Slope*-values within *LR* shows subtle jags (so-called *spikulae*) along the border of S_{large}.

The observations in this section could be validated by means of a report from an experienced radiologist who supposed that S_{small} forms a satellite lesion connected to S_{large} by one of the spikulae.

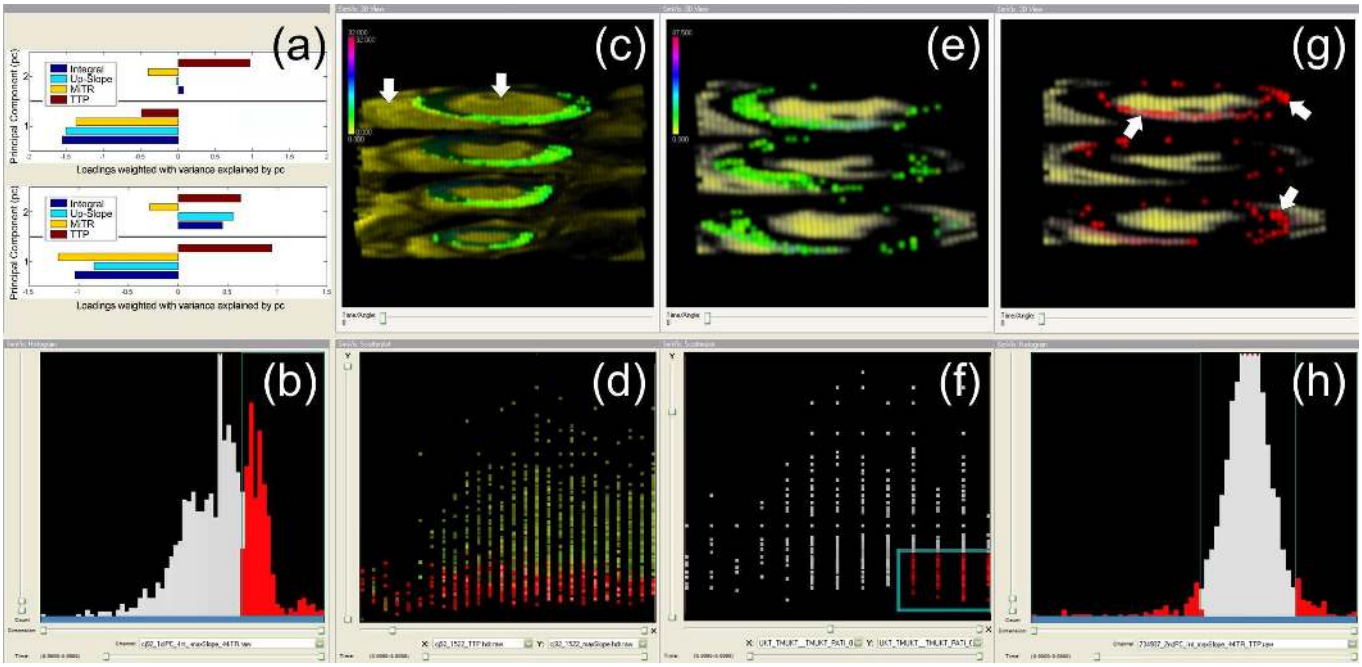

Fig. 7. Visual analysis in CHD diagnosis of datasets $Heart_1$ *(a-d)* and $Heart_2$ *(a, e-h)*. *(a):* Plot representing $pc1$ and $pc2$ of datasets $Heart_1$ (top) and $Heart_2$ (bottom). Brushing the scores of $pc1$ *(b)* reveals the infarcted region (green area in *(c)*). The right ventricle (left arrow) and the lumen (right arrow) are presented as context information. The selection from *(b)* is transferred to a scatterplot *(d)* opposing TTP (x-axis) and *Up-Slope* (y-axis). TTP is not a reliable parameter to detect the infarcted tissue in this case since the selection is spread over the entire codomain (red dots). However, this may not be valid for another dataset as illustrated in *(e-f)* for $Heart_2$. A selection of high TTP-values and small *Up-Slope*-values *(f)* reveals the infarcted tissue (green area in *(e)*). Brushing of $pc2$ *(h)* which represents an atypical enhancement pattern exhibits areas where the segmentation of the myocardium failed *(g)*.

4.3 CHD Diagnosis

In CHD diagnosis, the detection and localization of a perfusion deficit as well as the assessment of the severity are directly relevant for treatment decisions. Major diagnostic tasks to be performed are to evaluate whether the patient suffers from CHD, to evaluate the severity of the disease and to assess the vascular supply of less perfused tissue. At an early stage, CHD is characterized by a perfusion defect caused by a stenosis (an abnormal vessel narrowing). The localization of the perfusion defect with respect to the myocardium combined with anatomical knowledge about the supplying coronary arteries is essential in detecting stenosis as well as in early CHD diagnosis [28]. For CHD diagnosis, the parameters *Up-Slope, PE, TTP* and *Integral* have been approved [2],[30], and [29].

Case Study. The two patients, whose datasets will be analyzed in this subsection, both suffered from a heart attack. The matrix of dataset $Heart_1$ is: 144×192, slice distance: 18 mm, number of slices: 4, temporal resolution: 40 measurements in 2seconds. The matrix of dataset $Heart_2$ is: 144×192, slice distance: 18 mm, number of slices: 3, temporal resolution: 40 measurements in 2 seconds.

Statistical analysis. In a first step, $MiTR$ has been added to the initially suggested set of approved parameters. The examination of the correlation coefficients for $Heart_1$ and $Heart_2$ revealed a strong correlation between $Integral$ and PE. Since the variance of the $Integral$-values had been higher than the variance of the PE-values, in both cases, PE was excluded from the subsequent PCA.

The PCA of $Heart_1$ showed two major trends expressed by $pc1$ and $pc2$, respectively (Fig. 7 (a, upper plot)). Both pc's together explain $\approx 91\%$ of the variance in the data. However, $pc1$ describes an atypical enhancement pattern. In damaged tissue, the blood flow is delayed (high TTP-values) and diminished (e.g. low $Integral$-values). However, $pc1$ indicates a proportional relationship. This will be further examined in the visual analysis stage (see below).

The PCA of $Heart_2$ showed three major trends expressed by $pc1$ to $pc3$. All together account for $51\% + 25\% + 17\% = 93\%$ of the variance in the data. For the sake of brevity, only the first two pc's are examined here (Fig. 7 (a, lower plot)). A typical enhancement pattern is represented by $pc1$. However, $pc2$ shows an atypical pattern. As in $pc1$ of $Heart_1$, TTP is proportional to $Integral$ and *Up-Slope*. Furthermore, $MiTR$ is inversely proportional to *Up-Slope* though both parameters describe the steepness of the curve during wash-in.

Visual analysis. To examine the atypical enhancement pattern represented by $pc1$ of $Heart_1$, the scores of $pc1$ have been brushed in a histogram (Fig. 7 (b)). A selection of high values reveals the infarcted tissue (green region in Fig. 7 (c)) within the ring-shaped myocardium. Color mapping has been applied to encode the *Up-Slope*. Since the circular shape of the myocardium hampers the orientation, context information has been added. Two arrows point at the right ventricle (left arrow) and the lumen of the left ventricle (right arrow). Only now, anatomical knowledge about the correspondence between myocardial regions and supplying coronary arteries may be exploited. The selection from Fig. 7 (b) has been transferred for *multi-variate analysis* to a scatterplot opposing TTP (x-axis) and *Up-Slope* (y-axis) (red dots in Fig. 7 (d)). Interestingly, the infarcted tissue is spread over all timepoints. Probing the time-intensity curves within the infarcted region showed that the acquisition time of the scan was too short to determine a reliable TTP. In the infarcted region, no CA arrived at all over time. However, a PE and therefore a TPP always exist no matter if the time-intensity curve represents CA enhancement or only noise. After all, it seems that in spite of the unreliable TTP-values a brushing of $pc1$ still delivers meaningful results. This might be due to the low loading of TTP (Fig. 7 (a, upper plot)). However, the high *loading* of the unreliable TTP-values in $pc2$ prevents meaningful brushing results there.

One major difficulty in analyzing perfusion data is that a parameter that has been evaluated as unreliable in one case may turn out to be reliable in another case and vice versa. As illustrated in Fig. 7 (a, lower plot and e-f), TTP might be a reliable parameter for *feature localization* in $Heart_2$. Brushing of high TTP-values (x-axis) and small *Up-*

Slope-values (y-axis) reveals the infarcted region (green). Here, $pc1$ describes a typical enhancement pattern. In contrast, $pc2$ describes an atypical pattern: TTP and $Integral$ are proportional, and *Up-Slope* and $MiTR$ are inversely proportional related. Brushing of extreme values of $pc2$ (red bars in Fig. 7 (h)) reveals areas at the transition between myocardium and lumen and myocardium and pericardium (arrows in Fig. 7 (g)). Further examination of these areas showed that the propagation of the segmented myocardial contours over time did not match the myocardium at all time-points (recall Sec. 4). A prerequisite for a correct matching is a working motion-correction which failed partially.

5 Prior and Related Work

This section describes prior and related work on the application of InfoVis techniques for the analysis of multi-field data as well as on the visual analysis of perfusion data.

Visual Exploration of Multi-field Data. Our visualization concepts extend ideas from general systems for analyzing and exploring multidimensional image data such as [1]. Due to the absence of standardized intensity values and the high variability of image scanners and patient data, the analysis of perfusion is a typical exploratory analysis task where visual data mining techniques are essential [18].

Closely related concepts were presented by Gresh and Rogowitz in the WEAVE system [13]. In particular, we employ their concept of tightly integrating a 3D-visualization with multiple statistical representations, connected by brushing facilities applied to scatterplot representations. Similar to their exploratory scenarios, we also attempt to quickly compare and correlate variables. Inspired by their approach, Doleisch et al. developed the SimVis framework for interactive feature specification for CFD data in previous work [11][10]. In [5], the concepts of Gresh and Rogowitz have been optimized for interactive work with very large medical multi-field datasets and extended by the integration of analysis techniques from pattern classification. Henze [17] analyzed time-varying CFD data by multiple linked views. However, instead of analyzing the time-dependent data directly, we employ the perfusion parameters derived from them. Among the typical exploration techniques, linking and brushing is of crucial importance. Brushing refers to the graphical selection of data subsets which are emphasized and operated in various ways. The first comprehensive realization of this concept was presented in [3].

Visual Exploration of Perfusion Data. Basic visualization techniques for exploring perfusion data were described by [4] (focus on tumor perfusion) and [20] (focus on cerebral perfusion). The cinematic depiction of gray scale images in a movie loop gives an impression of the enhancement pattern [7]. *Subtraction images* depict the intensity difference between two selected points in time, thus, emphasizing regions where the CA is absorbed. However, they do not provide quantitative temporal and spatial information, which could make the diagnostic results more reproducible. Color-coded parameter maps [20] reveal the regional distribution of selected perfusion parameters. However, the analysis of parameter combinations in a tiled visualization requires a mental integration of suspicious regions.

Multiparameter visualizations, integrating several perfusion parameters in one image, were introduced in [19] and [28]. Different kinds of multivariate color scales, color icons and colored height fields are discussed. Flexible lenses were also used to integrate the visualization of a foreground parameter (in the lens region) with a background parameter. In particular for DCE-MRIM with its high spatial resolution, direct volume rendering techniques have been explored. A color-coded Closest Vessel Projection especially suitable for exploring DCE-MRIM data was presented in [19]. Coto et al. [8] employ Two-level volume rendering and importance driven volume rendering to focus volume rendered images to previously segmented breast lesions. This work is the closest to our work since also linking and brushing was employed to select regions of interest. However, they did not consider the perfusion parameters, described in Sect. 2.1. Instead, they considered only the intensity and the enhancement in a subtraction image. Also, their approach is dedicated to DCE-MRIM data. A rather general technique to support the visual exploration of high dimensional data was presented by [25]. Their *application profile flags* may be used to integrate time-intensity curves immediately in a visualization, thus supporting the mental integration of the curve parameters and the display of the original perfusion data. Finally, [16] describe highly interactive 3D visualizations of DCE-MRIM data in a virtual reality environment.

Analysis of Perfusion Data. Another venue of analyzing perfusion data relates to a statistical analysis as well as mining and knowledge discovery techniques. In particular, the classification of DCE-MRIM data by means of artificial neural networks and clustering techniques is an active research area [23, 6, 33]. As an example, Twellmann et al. [33] applied an artificial neural network (ANN) architecture which combines unsupervised and supervised techniques for voxel-by-voxel classification of temporal kinetic signals derived from DCE-MRIM data. Chen et al. [6] investigated and developed a fuzzy c-means (FCM) clustering-based technique for automatically identifying characteristic kinetic curves from segmented breast lesions in DCE-MRIM data. Nattkemper and Wissmueller [27] described the application of self-organized maps to time curve features of DCE-MRIM data and discussed how the results may be visually represented as color-coded cross-sections. Automatic classification may be useful in a screening setting in order to replace the opinion of a second radiologist or to direct a radiologist to suspicious regions.

6 Summary and Conclusion

We presented the integration of pre-processing techniques, statistical methods and interactive feature specification for the analysis of the multi-dimensional space of perfusion parameters, derived from medical perfusion data. The visual analysis strategy presented here allows to assess the reliability of specific perfusion parameters, the correlation of perfusion parameters in a particular case and thus enables an efficient evaluation focused on a significant subset of perfusion parameters. Compared to the prevailing purely visually and highly subjective evaluation methods, our approach enables a more reproducible evaluation supported by quantitative analysis results. Our research contributes to answering questions with respect to the diagnostic value of a certain combination of perfusion parameters. Such questions are debated in the medical research literature and they are difficult to treat, since the choice of specific imaging parameters strongly influences the diagnostic results. Thus, our visual analysis approach may be used to investigate the effects of a new contrast agent, a new scheme of contrast agent administration or changes in other imaging parameters on the diagnostic value of perfusion parameter combinations.

The most important work to be done relates to a thorough evaluation of the presented analysis strategy for a larger number of specific cases in cerebral, tumor, and myocardial perfusion. Within such an evaluation, the perfusion data analysis and clinical parameters characterizing the progress of the respective disease have to be integrated to better understand the diagnostic value of perfusion parameters. Based on such an evaluation, dedicated software systems for routine clinical diagnosis may be developed. Such systems must be fine-tuned to particular applications and should hide most of the analytical processes and instead present primarily the results of analytic processes together with a set of standardized visualizations.

With respect to the analysis strategy, the incorporation of clustering techniques which classify regions according to the similarity of time-intensity curves, deserves a systematic investigation. Based on recent progress, e.g., in kidney perfusion studies, such a classification may strongly enhance the user's task of selecting regions of interest.

Acknowledgements

We thank F. Grothues, A. Fessel (Medical Faculty, University of Magdeburg), J. Wiener (Boca Raton Comm. Hosp., Florida), M. Fenchel, S. Miller and A. Seeger (Max Planck MR-Center, University Tübingen) for providing the image data our work is based on. We are grateful to MeVis Research for providing advanced Me*VisLab*-features. This work has been partly funded by the "Bridge" funding program of the Austrian Funding Agency (FFG) in the scope of the Severe Weather Explorer project (Nr. 812122).

REFERENCES

[1] C. Ahlberg and E. Wistrand. IVEE: An Information Visualization and Exploration Environment. In *IEEE Information Visualization*, pages 66–73, 1995.

[2] N. Al-Saadi, M. Gross, A. Bornstedt, B. Schnackenburg, C. Klein, E. Fleck, and E. Nagel. Comparison of various parameters for determining an index of myocardial perfusion reserve in detecting coronary stenosis with cardiovascular magnetic resonance tomography. *Z Kardiol*, 90(11):824–34, Nov 2001.

[3] R. A. Becker and W. S. Cleveland. Brushing scatterplots. *Technometrics*, 29(2):127–142, 1987.

[4] U. Behrens, J. Teubner, C. J. Evertsz, M. Walz, H. Jürgens, and H.-O. Peitgen. Computer-Assisted Dynamic Evaluation of Contrast-Enhanced-MRI. In *Proc. of Computer Assisted Radiology*, pages 362–367, 1996.

[5] J. Blaas, C. Botha, and F. Post. Interactive visualization of multi-field data using dynamically linked physical and feature space views. EuroVis, 2007.

[6] W. Chen, M. Giger, U. Bick, and G. Newstead. Automatic identification and classification of characteristic kinetic curves of breast lesions on DCE-MRI. *Medical Physics*, 33(8):2878–2887, 2006.

[7] P. L. Choyke, A. J. Dwyer, and M. V. Knopp. Functional tumor imaging with dynamic contrast-enhanced magnetic resonance imaging. *J Magn Reson Imaging*, 17(5):509–20, May 2003.

[8] E. Coto, S. Grimm, S. Bruckner, E. Gröller, A. Kanitsar, and O. Rodriguez. MammoExplorer: An Advanced CAD Application for Breast DCE-MRI. In *Proc. Vision, Modelling, and Visualization (VMV)*, pages 91–98, 2005.

[9] J. A. den Boer and P. J. M. Folkers. MR perfusion and diffusion imaging in ischaemic brain disease. *Medica Mundi*, 41(2):20–35, 1997.

[10] H. Doleisch, M. Gasser, and H. Hauser. Interactive feature specification for focus+context visualization of complex simulation data. In *Proc. of the 5th Joint IEEE TCVG - EUROGRAPHICS Symposium on Visualization (VisSym 2003)*, pages 239–248, Grenoble, France, May 2003.

[11] H. Doleisch and H. Hauser. Smooth brushing for focus+context visualization of simulation data in 3D. *Journal of WSCG*, 10(1):147–154, 2002.

[12] G. Furnas. Generalized fisheye views. In *Proc. of the ACM CHI '86 Conf. on Human Factors in Computing Systems*, pages 16–23, 1986.

[13] D. L. Gresh, B. E. Rogowitz, R. L. Winslow, D. F. Scollan, and C. K. Yung. WEAVE: A System for Visually Linking 3-D and Statistical Visualizations, Applied to Cardiac Simulation and Measurement Data. In *IEEE Visualization*, pages 489–492, 2000.

[14] H. K. Hahn and H.-O. Peitgen. The skull stripping problem in MRI solved by a single 3d watershed transform. In *miccai*, volume 1935 of *LNCS*, pages 134–143. Springer, 2000.

[15] H. Hauser. Generalizing focus+context visualization. In *Scientific Visualization: The Visual Extraction of Knowledge from Data*, pages 305–327, 2005.

[16] G. Hellwig, G. Brix, J. Griebel, R. Lucht, S. Delorme, M. Siebert, and K.-H. Englmeier. Dynamic MR mammography: three-dimensional real-time visualization of contrast enhancement in virtual reality. *Academic Radiology*, 9:1255–1263, 2002.

[17] C. Henze. Feature detection in linked derived spaces. In *IEEE Visualization*, pages 87–94, 1998.

[18] D. A. Keim. Information visualization and visual data mining. *IEEE Trans. Vis. Comput. Graph.*, 8(1):1–8, 2002.

[19] S. Kohle, B. Preim, J. Wiener, and H.-O. Peitgen. Exploration of Time-varying Data for Medical Diagnosis. In *Proc. of Vision, Modeling, and Visualization*, pages 31–38. Aka, 2002.

[20] M. König, E. Klotz, and L. Heuser. Perfusion CT in Acute Stroke: Characterization of Cerebral Ischemia using Parameter Images of Cerebral Blood Flow and their Therapeutic Relevance. *Electromedica*, 66(2):61–67, 1998.

[21] M. König, E. Klotz, and L. Heuser. [Cerebral perfusion CT: theoretical aspects, methodical implementation and clinical experience in the diagnosis of ischemic cerebral infarction]. *Rfo*, 172(3):210–8, Mar 2000.

[22] C. K. Kuhl, P. Mielcareck, S. Klaschik, C. Leutner, E. Wardelmann, J. Gieseke, and H. H. Schild. Dynamic Breast MR Imaging: Are Signal Intensity Time Course Data Useful for Differential Diagnosis of Enhancing Lesions? *Radiology*, 211(1):101–110, 1999.

[23] R. E. Lucht, M. V. Knopp, and G. Brix. Classification of signal-time curves from dynamic MR mammography by neural networks. *Magnetic Resonance Imaging*, 19(1):51–57, 2001.

[24] M. Lysaker, A. Lundervold, and X. Tai. Noise Removal Using Fourth-Order Partial Differential Equation with Applications to Medical Magnetic Resonance Images in Space and Time. *IEEE Transactions on Image Processing*, 12(12):1579–1590, 2003.

[25] M. Mlejnek, P. Ermes, A. Vilanova, R. van der Rijt, H. van den Bosch, E. Gröller, and F. Gerritsen. Application-oriented extensions of profile flags. In *Data Visualization (Proc. of Eurographics/IEEE Symposium on Visualization)*, pages 339–346, 2006.

[26] W. Müller, T. Nocke, and H. Schumann. Enhancing the visualization process with principal component analysis to support the exploration of trends. In *APVis '06: Proceedings of the 2006 Asia-Pacific Symposium on Information Visualisation*, pages 121–130, 2006.

[27] T. Nattkemper and A. Wismuller. Tumor feature visualization with unsupervised learning. *Medical Image Analysis*, 9(4):344–351, 2005.

[28] S. Oeltze, F. Grothues, A. Hennemuth, A. Ku, and B. Preim. Integrated Visualization of Morphologic and Perfusion Data for the Analysis of Coronary Artery Disease. In *Eurographics / IEEE VGTC Symposium on Visualization*, pages 131–138, 2006.

[29] I. Paetsch, C. Jahnke, A. Wahl, R. Gebker, M. Neuss, E. Fleck, and E. Nagel. Comparison of Dobutamine Stress Magnetic Resonance, Adenosine Stress Magnetic Resonance, and Adenosine Stress Magnetic Resonance Perfusion. *Circulation*, 110(7):835–842, 2004.

[30] J. R. Panting, P. D. Gatehouse, G. Z. Yang, M. Jerosch-Herold, N. Wilke, D. N. Firmin, and D. J. Pennell. Echo-planar magnetic resonance myocardial perfusion imaging: parametric map analysis and comparison with thallium SPECT. *J Magn Reson Imaging*, 13(2):192–200, Feb 2001.

[31] D. Rueckert, L. Sonoda, C. Hayes, D. Hill, M. Leach, and D. J. Hawkes. Nonrigid registration using free-form deformations: application to breast MR images. *IEEE Trans. Med. Imag.*, 18(8):712–721, 1999.

[32] A. Schenk, G. Prause, and H.-O. Peitgen. Efficient semiautomatic segmentation of 3d objects in medical images. In *MICCAI*, pages 186–195. Springer, 2000.

[33] T. Twellmann, O. Lichte, and T. Nattkemper. An adaptive tissue characterization network for model-free visualization of dynamic contrast-enhanced magnetic resonance image data. *IEEE Trans. Med. Imag.*, 24(10):1256–1266, 2005.

[34] M. Ward. XmdvTool: integrating multiple methods for visualizing multivariate data. In *VIS '94: Proceedings of the conference on Visualization '94*, pages 326–333. IEEE Computer Society Press, 1994.